1-1-2005

High-Temperature Creep-Deformation Behavior of the Ni-Based Superalloy M963

Hongtao Zhu
University of Wollongong, hongtao@uow.edu.au

Cheng Lu
University of Wollongong, chenglu@uow.edu.au

A K. Tieu
University of Wollongong, ktieu@uow.edu.au

Lizi He
University of Wollongong

Q. Zheng
Chinese Academy of Science

See next page for additional authors

High-Temperature Creep-Deformation Behavior of the Ni-Based Superalloy M963

L.Z. HE, Q. ZHENG, X.F. SUN, H.R. GUAN, Z.Q. HU, A.K. TIEU, C. LU, and H.T. ZHU

The high-temperature creep-deformation behavior of a Ni-based M963 superalloy has been investigated over a broad stress range of 80 to 600 MPa at high temperatures (800 °C to 975 °C). The detailed dislocation configurations at different creep stages are examined through transmission electron microscopy (TEM). The results show that the deformation mechanism is stress and temperature dependent and mainly consists of three dislocation-controlling mechanisms: stacking faults and dislocation-pair shearing, dislocation bowing and Orowan looping, and dislocation climb.

I. INTRODUCTION

NI-BASED superalloys are mainly strengthened by γ' precipitates and solution additions and are produced in various forms suitable for application at high temperature, due to their excellent creep and fatigue strength and good corrosion resistance. At high temperature, the life of turbine blades and vanes is controlled by creep deformation and damage processes of the materials.[1] Extensive research has been focused on investigating the creep behavior of some commercial Ni-based superalloys, including the effects of minor elements (such as C, B, and Zr),[2,3,4] the environment,[5,6,7] γ'-rafting,[8–12] dislocation structures,[13–18] creep-fatigue behavior,[19,20,21] *etc*. The M963 alloy, a polycrystalline Ni-based superalloy, is being used as a material for blades and vanes in gas-turbine engines. It has a chemical composition and microstructure similar to those of the Ni-based superalloy Mar-M200. Due to its relatively high contents of refractory elements such as tungsten, molybdenum, titanium, niobium, *etc*., it has been reported that the alloy has intermediate-temperature brittleness,[22] and some efforts have been made to improve this behavior.[23,24] Investigating the creep-deformation mechanism can benefit the efforts to develop high-temperature alloys, to achieve more-resistant alloys, and to rationalize the creep behavior of these alloys. Until now, the high-temperature creep properties of the M963 superalloy have not been published. The purpose of the present work is to explore in detail the creep behavior under constant load at different temperatures and stresses and to gain a deeper understanding of the high-temperature creep-deformation mechanisms of the M963 superalloy.

II. EXPERIMENTAL PROCEDURE

The chemical composition of the M963 alloy used in this work is given in Table I. The minor elements are 8 wt ppm P, 10 wt ppm S, 3 wt ppm O, and 6 wt ppm N. The master alloy was remelted and cast into test bars, which were then solution treated at 1210 °C for 4 hours, followed by air cooling. The solution-treated microstructure consists of a γ matrix, γ' precipitate, $\gamma + \gamma'$ eutectic, and MC and M_6C carbides. The γ' particles at dendrite cores have an average size of 0.1 μm and volume fraction of 42 pct, approximately.

Creep specimens were machined from solution-treated bars measuring 10 mm in diameter and 50 mm in gage length. The constant-load tensile-creep tests were conducted in air over the 80 to 600 MPa stress range from 800 °C to 975 °C. The temperature was measured using three thermocouples attached to the gage part of each specimen and was controlled within ±2 °C during all creep tests. The inductive transducers could detect strain variations as small as 10^{-4}, and the output was automatically shown at any time. Most samples were run to failure, and some were interrupted for dislocation observations.

Dislocation-configuration observation was carried out using a PHILIPS* EM420 transmission electron microscope (TEM) at 120 kV. A thin-foil sample was prepared by twin-jet thinning electrolytically in a solution of 7 vol pct perchloric acid in alcohol at −30 °C.

*PHILIPS is a trademark of Philips Electronic Instruments Corp., Mahwah, NJ.

III. RESULTS AND DISCUSSION

A. *Creep Curves*

The creep curves of strain (ε) *vs* time (t) at different temperatures are shown in Figure 1. It can be seen that the shape of the creep curve exhibits strong temperature and stress dependence. In the low-temperature region (800 °C), the creep curves show an obvious primary creep stage, followed by a dominant steady-state creep stage and then an extended accelerating creep stage leading to failure. With decreasing applied stress, the steady-state creep stage is prolonged (Figure 1(a)). In the high-temperature region (900 °C and 975 °C), the creep curves take on a very short primary stage (Figures 1(b) and (c)). The same effect of the applied stress on creep curves is also observed at high temperatures.

For metals and alloys at high temperatures, the dependence of the steady-state creep rate ($\dot{\varepsilon}_{ss}$) on the applied stress (σ_a) and temperature (T) can be usually describe as a power law:[25]

$$\dot{\varepsilon}_{ss} = A\sigma_a^n \exp(-Q_c/RT) \quad [1]$$

L.Z. HE, formerly Postdoctoral Student, with the Institute of Metal Research, Chinese Academy of Sciences, is Visiting Fellow, Mechanical Engineering Department, University of Wollongong. Contact e-mail: cybhlz@163.net Q. ZHENG, Senior Engineer, X.F. SUN and H.R. GUAN, Professors, and Z.Q. HU, Professor and Member of Chinese Engineering Academy, are with the Institute of Metal Research, Chinese Academy of Sciences, Shenyang, 110016, People's Republic of China. A.K. TIEU, Professor, and C. LU and H.T. ZHU, Research Fellows, are with Mechanical Engineering Department, University of Wollongong, Wollongong, NSW2522, Australia.

Manuscript submitted January 4, 2005.

Table I. Chemical Composition of the M963 Alloy (Weight Percent)

C	Cr	Al	Ti	Mo	W	Co	Nb	Zr	B	Ce	Y	Ni
0.15	8.89	6.00	2.55	1.64	10.10	10.01	1.10	0.031	0.03	0.02	0.01	bal

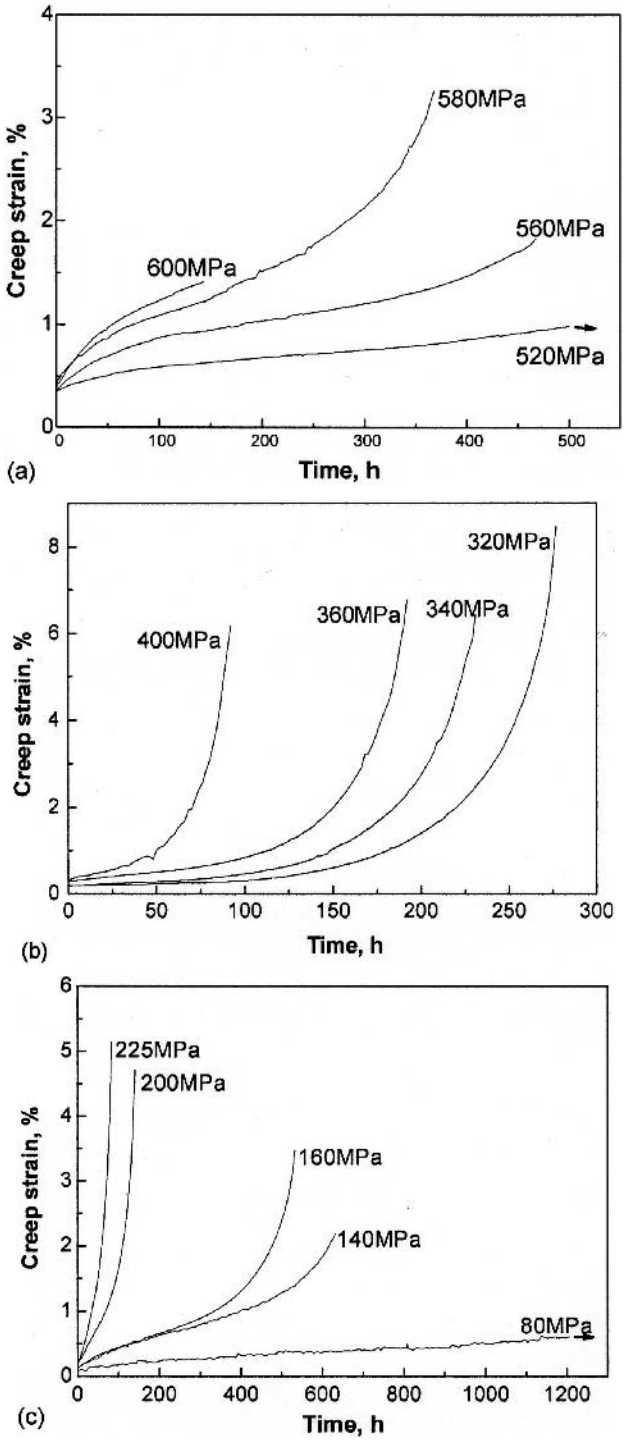

Fig. 1—Creep curves for the M963 alloy at different temperatures and stresses: (*a*) 800 °C and 520 MPa, 560 MPa, 580 MPa, and 600 MPa, (*b*) 900 °C and 320 MPa, 340 MPa, 360 MPa, and 400 MPa, and (*c*) 975 °C and 80 MPa, 140 MPa, 160 MPa, 200 MPa, and 225 MPa.

where A is a constant for a given material, n is the apparent stress exponent, Q_c is the apparent activation energy for creep, and R is the gas constant. For pure metals and simple alloys, the value of n is between 4 and 6, while the value of Q_c is close to that for self-diffusion (Q_{sd}). Figure 2 shows the change of the steady-state creep rate with testing temperature. The data obtained at each temperature appear to lie on a straight line, and the n value is calculated from the slopes. For the M963 superalloy, the n value is 9.5 at the low temperature (800 °C), which is higher than the theoretical values mentioned previously, and it is about 4.0 at the high temperatures (900 °C and 975 °C). The change in n value indicates that the different creep-deformation mechanisms may operate at different temperatures. The much higher n value was also observed in other particle-strengthened superalloys,[26–29] and the effect of temperature and stress on the apparent activation energy will be discussed in another work by the authors.

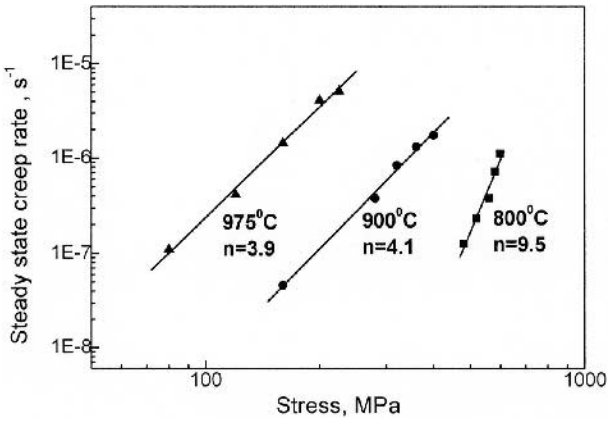

Fig. 2—The stress dependence of the steady-state creep rate of the M963 alloy at different temperatures.

B. *Primary Creep Stage*

Figure 3 shows the typical heat-treated microstructure of the M963 alloy. The fine cubic γ' precipitates are separated by narrow γ channels. A consistent crystal structure (fcc) and lattice constant (about 0 to 1 pct mismatch) between the γ' and γ phases allow homogeneous nucleation of precipitates with a low surface energy and long-term stability. The γ' phase, having an ordered $L1_2$ structure, contributes antiphase boundary (APB) strengthening to the alloys.

The dislocation configurations of the primary creep stage at different temperatures and stresses are illustrated in Figure 4. At this stage, deformation is very inhomogeneous, tangled γ-γ' interface dislocations are observed at local regions, and the dislocations increase by bowing between γ' precipitates (Figures 4(a) through (d)). It should be noted that the γ' precipitates still retain their cubic shape. Different directional slip of {111} <110> systems in the γ channels can be found (Figure 4(b)). At 900 °C and 400 MPa, some matrix dislocations bowing between γ' precipitates and others cutting through γ' particles by stacking-fault formation and APB-coupled dislocation pairs are seen in

Figure 4(c). Since the intrinsic stacking faults are lying on a common (111) glide plane, the matrix dislocations must, as totals, dissociate into partials at the γ-γ' interface, producing a single superpartial gliding in the γ' phase and a partial left at the interface, which relaxes the high-coherency stresses at the γ-γ' interface. Therefore, the partial reduces the overall energy of the dislocation the interface configuration, so that a stacking-fault formation can be generated at a coherent interface. After passing the precipitate, the partial dislocations rearrange themselves to totals for further motion in the matrix. Groups of partial dislocations may create a variety of fault configurations in γ' precipitates. Kear *et al.*[30] suggested the requirement of coherent interfaces for stacking-fault formation. Otherwise, the resulting pileups of matrix dislocations at the interfaces generate local stresses and cause a transition from a stacking fault to an APB mechanism. The existence of the stacking faults in the specimen crept at 900 °C/400 MPa indicates that dislocations move by shearing γ' particles at stresses as high as 400 MPa. The distribution of dislocations at 975 °C/160 MPa is still inhomogeneous, but the dislocation density increases (Figure 4(d)). At the high temperature, the diffusion-controlled processes are evident; dislocations are mobile through the mechanism of climb and additional slip systems are introduced with increasing temperature, so the dislocation density increases rapidly with plastic deformation during creep.[31] Kolbe *et al.*[14] discovered that dislocation networks at the γ-γ' interface are the typical microstructures for the primary creep stage after shear-creep

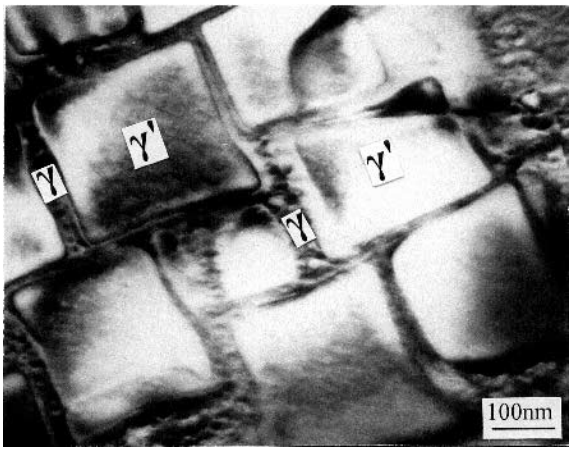

Fig. 3—TEM image showing the standard heat-treated microstructure (1210 °C/4 h and air cooled) and **g** = <200>.

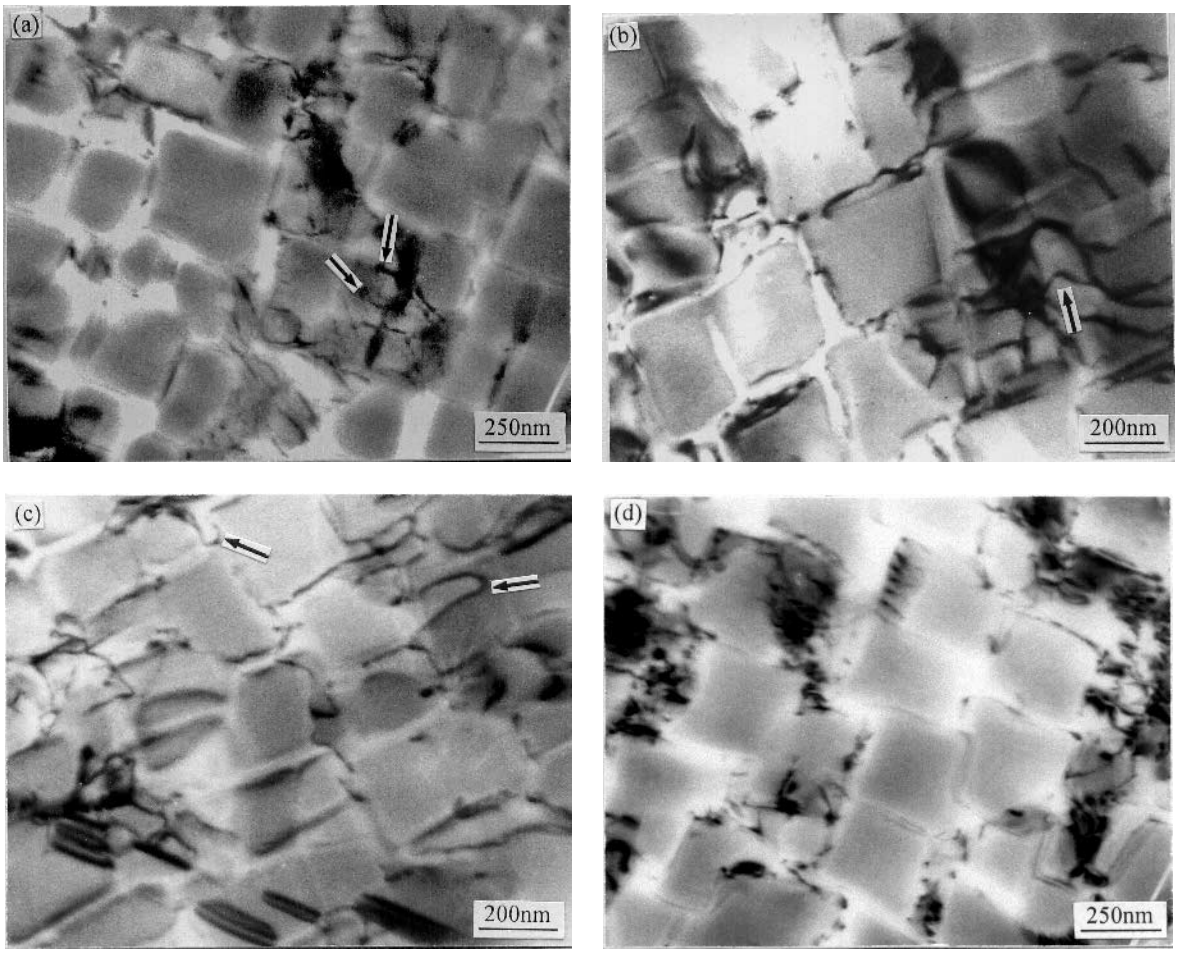

Fig. 4—TEM images showing dislocation configurations of the M963 alloy at the primary creep stage and **g** = <200>: (*a*) 800 °C/560 MPa for 10 h (ε = 0.88 pct), (*b*) 900 °C/320 MPa for 1 h (ε = 0.19 pct), (*c*) 900 °C/400 MPa for 1 h (ε = 0.33 pct), and (*d*) 975 °C/160 MPa for 1 h (ε = 0.13 pct).

deformation in a CMSX6 single-crystal Ni-based superalloy at 1025 °C/85 MPa. Due to the relatively low testing temperatures in the present work, the dislocation networks cannot be observed at the primary creep stage.

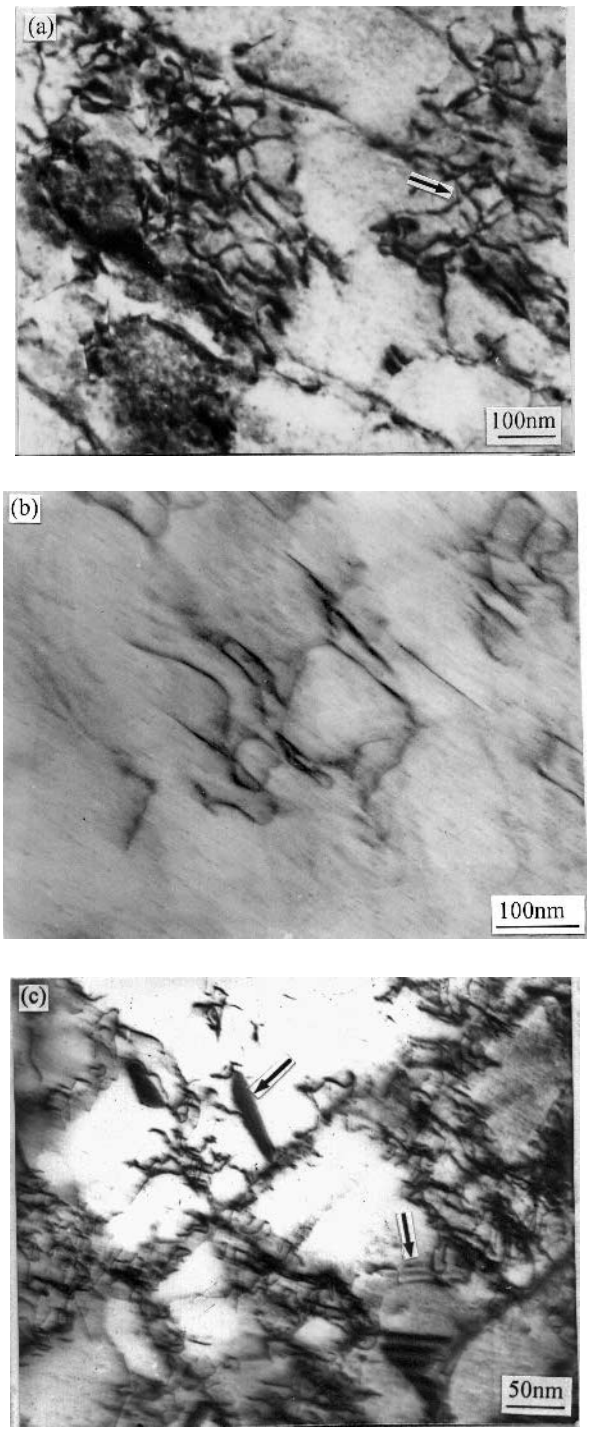

Fig. 5—TEM images showing dislocation configurations of the M963 alloy at the steady-state creep stage at 800 °C/560 MPa and $\mathbf{g} = <111>$: (*a*) dislocation regulation at the early stage (t = 130 h and ε = 0.92 pct), (*b*) dislocation loops at the middle stage (t = 250 h and ε = 1.11 pct), and (*c*) stacking-fault formation at the final stage (t = 310 h and ε = 1.22 pct).

C. *Steady-State Creep Stage*

The dislocation configurations of steady-state creep at different temperatures and stresses are shown in Figures 5 through 8. At 800 °C and the initial stage of steady-state creep (800 °C/560 MPa/130 hours), the tangled dislocations in γ channels at the local region (as marked by the arrow in Figure 5(a)) start to regulate. More detailed observations reveal that Orowan dislocation loops around γ' precipitates are frequently visible in the specimens interrupted in the middle of steady-state creep (Figure 5(b)). Such dislocation loops are produced in the process of dislocation bypass. The looping stress depends on the size and spacing of precipitates that change due to aging during creep tests. A small mean surface-to-surface spacing between γ' precipitates restricts dislocation motion significantly, whereas a larger one promotes homogeneous slip through a/2<110> dislocation bowing and looping.[32] Mukheji *et al*.[33] found that the γ'-precipitates spacing increased with increasing testing time and applied strain in the single-crystal SC16 superalloy. The Orowan looping stress decreased with the increment of particle spacing. At the final stage of steady-state creep, high-density tangled dislocations are trapped in γ channels, and stacking faults cutting γ' precipitates are also observed (Figure 5(c)). The local high-stress concentrations push leading dislocations at the γ-γ' interface into γ' precipitates by stacking faults.

In the high-temperature and high-stress range, the dislocation bowing between γ' precipitates and a few closed loops around the γ' precipitates are frequently seen in the specimens crept at 900 °C/400 MPa, as shown in Figure 6. The bypass dislocations usually form loops and tangles, and the dislocation density in the specimen may increase rapidly with plastic deformation during creep.

In the high-temperature and low-stress range, the stress values are less than those required for dislocation bowing or looping around precipitates, and dislocation climb is achieved through a jogging movement directly along the dislocation line, as shown by arrow A in Figure 7(a). The initial cubic γ' precipitates become elongated (rafting). Deformation is mostly confined within the γ matrix, leading to a homogeneous dislocation distribution; well-developed dislocation

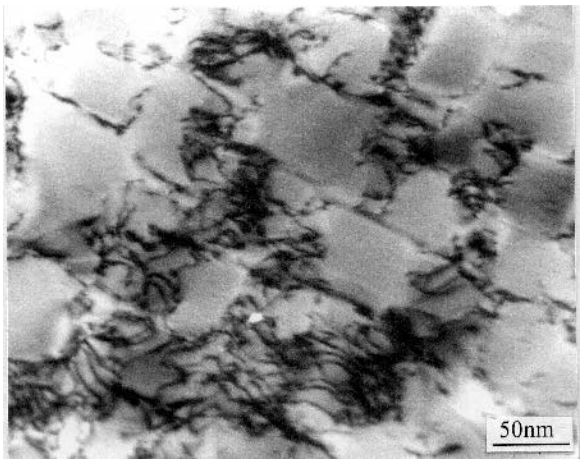

Fig. 6—TEM image showing the dislocation configuration of the M963 alloy at the steady-state creep stage at 900 °C/400 MPa, t = 20 h, ε = 0.5 pct, and $\mathbf{g} = <111>$.

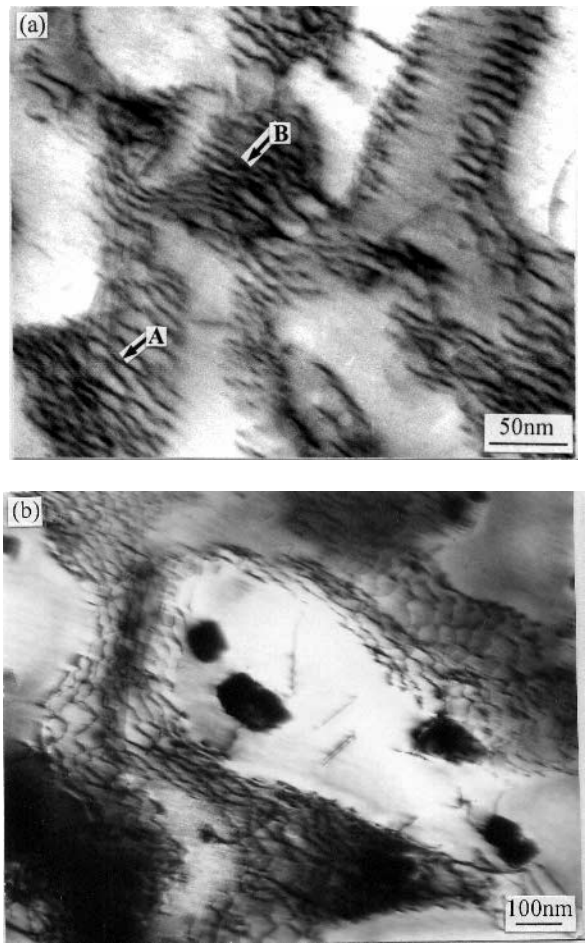

Fig. 7—TEM images showing dislocation configurations of the M963 alloy at the steady-state creep stage at 900 °C/320 MPa and **g** = <111>: (*a*) t = 80 hours and ε = 0.27 pct, and (*b*) t = 139 h and ε = 0.51 pct.

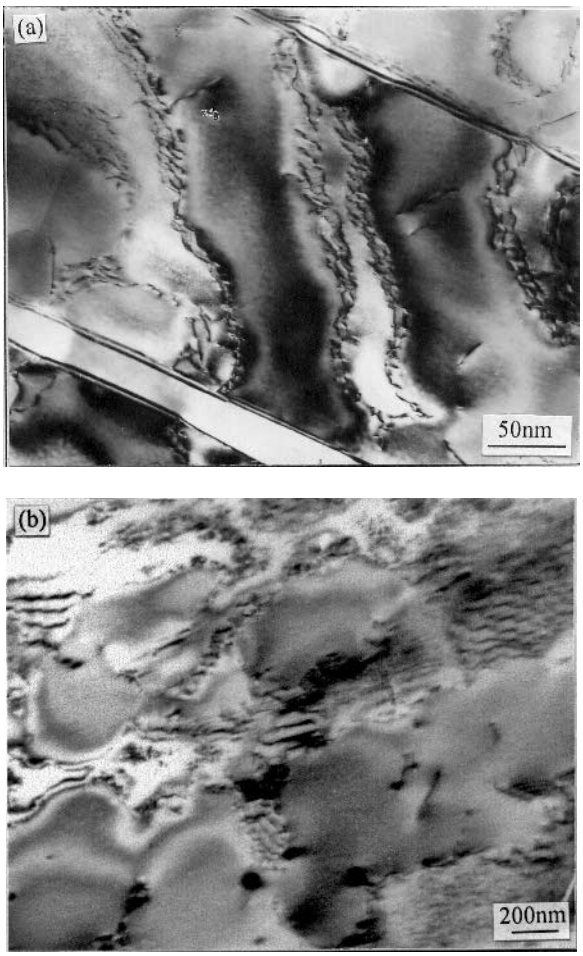

Fig. 8—TEM images showing dislocation configurations of the M963 alloy at the steady-state creep stage at 975 °C/160 MPa and **g** = <111>: (*a*) t = 100 h and ε = 0.44 pct, and (*b*) t = 300 h and ε = 0.89 pct.

networks start to form at the γ-γ' interface. Two sets of roughly parallel dislocations take place in the reaction to form a three-dimensional network at the γ-γ' interface marked by arrow B in Figure 7(a). Further, with the prolongation of the creep time, the networks gradually increase in number and lessen in size, leading to the formation of the stable network structure. As shown in Figure 7(b), the rafted γ' precipitates have been enveloped by the hexagonal dislocation network, and a large number of dislocations are piled up in γ channels. The dislocation networks are completely developed, and some dislocations cutting into the rafted γ' precipitates are observed in the specimens creep tested at 975 °C/160 MPa for 100 hours (Figure 8(a)). As the creep time is prolonged, the number of dislocations observed in the γ' precipitates increases (Figure 8(b)).

At the steady-state creep stage, the strain rate remains constant from the balance between strain hardening (network refinement due to dislocation glide) and recovery (network coarsening due to diffusion-controlled climb and the subsequent annihilation of dislocations). Several models have been proposed for the recovery of dislocations in the matrix of alloys.[34,35,36] Glide and recovery of dislocations inside γ' precipitates that impede dislocation motion and enhance the high-temperature strength of the Ni-based superalloys are the effective strengthening mechanisms.

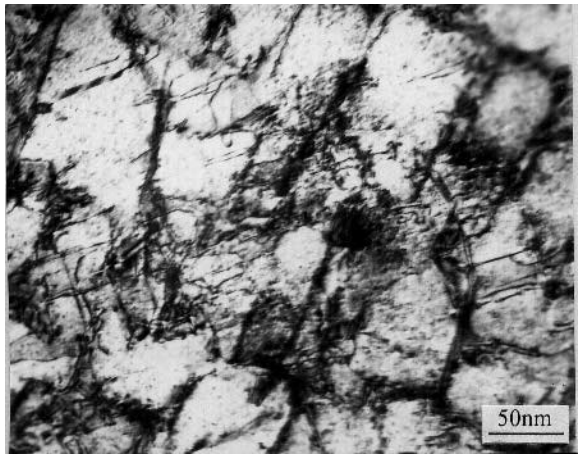

Fig. 9—TEM images showing stacking faults and dislocation pairs shearing γ' precipitates at the accelerating creep stage at 800 °C/560 MPa, t = 450 h, ε = 1.83 pct, and **g** = <200>.

D. *Accelerating Creep Stage*

Figure 9 shows the dislocation configurations at the accelerating stage of creep at 800 °C/560 MPa for 450 hours; stacking faults and dislocation pairs cutting into γ' precipitates are observed.

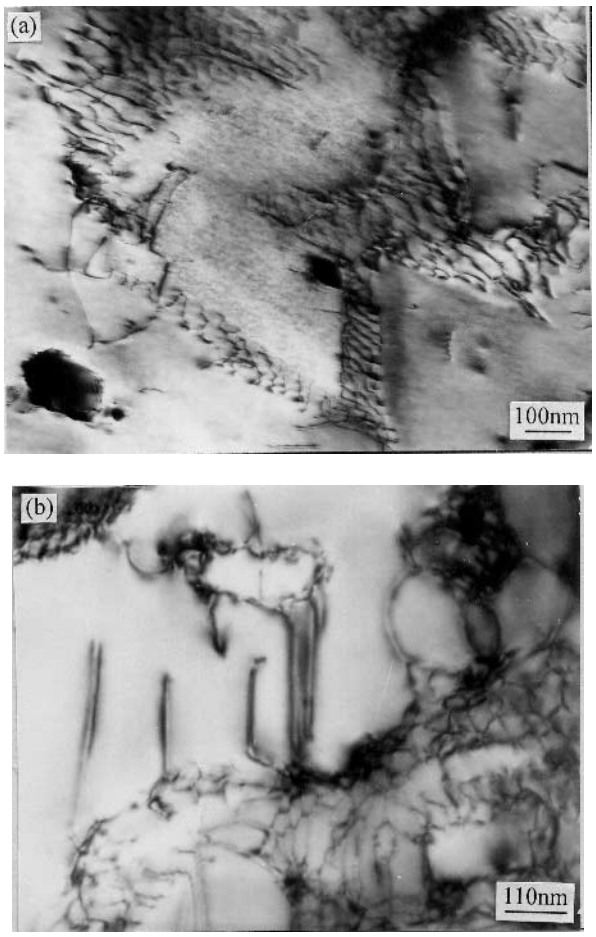

Fig. 10—TEM images showing broken dislocation networks at the accelerating creep stage and **g** = <200>: (*a*) 900 °C/320 MPa, t = 277 h and ε = 8.48 pct, and (*b*) 975 °C/160 MPa, t = 450 h and ε = 1.70 pct.

At high temperature, the rafted γ' precipitates are cut from the region, where the networks are damaged (Figure 10(a)). The morphology of the rafted γ' precipitates sheared by the <110> dislocations from the regions of the damaged networks is shown in Figure 10(b).

At the accelerating creep stage, high stress concentrations drive the leading dislocations cutting γ' precipitates by stacking faults and dislocation pairs at low temperatures. However, the rafted γ' precipitates have coarsened when creep enters the accelerating stage at high temperature. Most dislocation networks are still present at the γ-γ' interface, while others are locally damaged in the later period of creep. The damaged networks lose their coordinated role in maintaining the dynamic equilibrium, so that a large number of dislocations are piled up at some regions where the networks have been damaged, giving rise to the local stress concentration. Thereby, the matrix dislocations may cut into the rafted γ' precipitates from the interfaces.

V. CONCLUSIONS

During primary creep, the main deformation mechanism is dislocation bowing between γ' precipitates. At high stress, stacking faults cutting γ' precipitates is also observed.

During steady-state creep, deformation mechanisms have a high correlation with the testing temperature and applied stress. At low temperatures, dislocation bowing and Orowan looping are frequently visible, and stacking faults are also observed in γ' precipitates with increasing exposure time. In the high-temperature and high-stress range, a bypass mechanism involving dislocation bowing and Orowan looping occur. In the high-temperature and low-stress range, the dislocations climb and dislocation networks at the γ-γ' interface are formed. With increasing exposure time, dislocations in γ' precipitates are found.

During accelerating creep, staking faults and dislocation pairs cutting γ' precipitates occur at low temperatures; the shearing of γ' rafts by dislocations at damaged networks is observed at high temperatures.

REFERENCES

1. F.R.N. Nabarro and H.L. de Villiers: *The Physics of Creep*, Taylor and Francis, London, 1995, p. 83.
2. L.R. Liu, T. Jin, N.R. Zhao, Z.H. Wang, X.F. Sun, H.R. Guan, and Z.Q. Hu: *Mater. Sci. Eng. A*, 2003, vol. 361, pp. 191-97.
3. L.R. Liu, T. Jin, N.R. Zhao, Z.H. Wang, X.F. Sun, H.R. Guan, and Z.Q. Hu: *Mater. Sci. Eng. A*, 2004, vol. 385, pp. 105-12.
4. Q.Z. Chen, C.N. Jones, and D.M. Knowles: *Mater. Sci. Eng. A*, 2004, vol. 385, pp. 402-18.
5. X.B. Liu, B. Kang, W. Carpenter, and E. Barbero: *J. Mater. Sci*., 2004, vol. 39, pp. 1967-73.
6. U. Krupp, R. Orosz, H.J. Christ, U. Buschmann, and W. Wiechert: *Mater. Sci. Forum*, 2004, vols. 461–464, pp. 37-43.
7. S. Dryepondt, E. Andrieu, D. Monceau, F. Crabos, and C. Vernault: *Mater. Sci. Forum*, 2004, vols. 461–464, pp. 647-54.
8. G. Magadi and V.M. Radhakrishnan: *J. Mater. Eng. Performance*, 2004, vol. 13, pp. 493-503.
9. A. Jacques and P. Bastie: *Phil. Mag*., 2003, vol. 83, pp. 3005-27.
10. M. Kamaraj, K. Serin, M. Kolbe, and G. Eggeler: *Mater. Sci. Eng. A*, 2001, vol. 319, pp. 796-99.
11. S.G. Tian, C.R. Chen, J.H. Zhang, H.C. Yang, X. Wu, Y.B. Xu, and Z.Q. Hu: *Mater. Sci. Technol*., 2001, vol. 17, pp. 736-44.
12. R.C. Reed, N. Matan, D.C. Cox, M.A. Rist, and C.M.F. Rae: *Acta Mater*., 1999, vol. 47, pp. 3367-81.
13. M. Kolbe, K. Neuking, and G. Eggeler: *Mater. Sci. Eng. A*, 1997, vol. 234, pp. 877-79.
14. M. Kolbe, A. Dlouhy, and G. Eggeler: *Mater. Sci. Eng. A*, 1998, vol. 246, pp. 133-42.
15. V. Sass and M. Feller-Kniepmeier: *Mater. Sci. Eng. A*, 1998, vol. 245, pp. 19-28.
16. S. Nategh and S.A. Sajjadi: *Mater. Sci. Eng. A*, 2003, vol. 339, pp. 103-08.
17. A.C. Picasso, A.J. Marzocca, and I. Alvarez: *Mater. Sci. Eng. A*, 1997, vol. 234, pp. 1099-1102.
18. R. Srinivasan, G.F. Eggeler, and M.J. Mills: *Acta Mater*., 2000, vol. 48, pp. 4867-78.
19. T. Tong, S. Dalby, J. Byrne, M.B. Henderson, and M.C. Hardy: *Int. J. Fatigue*, 2001, vol. 23, pp. 897-902.
20. M. Okazaki and Y. Yamazaki: *Int. J. Fatigue*, 1999, vol. 21, pp. S79-86.
21. L.J. Chen, G. Yao, J.F. Tian, Z.G. Wang, and H.Y. Zhao: *Int. J. Fatigue*, 1998, vol. 20, pp. 543-48.
22. C. Yuan, X.F. Sun, F.S. Yin, H.R. Guan, Z.Q. Hu, Q. Zheng, and Y. Yu: *J. Mater. Sci. Technol*., 2001, vol. 17, pp. 425-28.
23. F.S. Yin, X.F. Sun, J.G. Li, H.R. Guan, and Z.Q. Hu: *Scripta Mater*., 2003, vol. 48, pp. 425-29.
24. L.Z. He, Q. Zheng, X.F. Sun, G.C. Hou, H.R. Guan, and Z.Q. Hu: *Mater. Sci. Eng. A*, 2004, vol. 380, pp. 340-48.
25. J.H. Gittus: *Creep Viscoelasticity and Creep Fracture in Solids*, Applied Science, London, 1975, p. 473.
26. K.R. Williams and B. Wilshire: *Met. Sci. J*., 1973, vol. 7, pp. 176-79.
27. P.W. Davis, G. Nelmes, K.R. Williams, and B. Wilshire: *Met. Sci. J*., 1973, vol. 7, pp. 87-92.
28. R.W. Lund and W.D. Nix: *Acta Metall*., 1976, vol. 24, pp. 469-81.

29. J.H. Haysselt and W.D. Nix: *Acta Mater*., 1977, vol. 25, pp. 595-607.
30. B.H. Kear, J.M. Oblak, and A.F. Giamei: *Metall. Trans. A*, 1970, vol. 1, pp. 2477-86.
31. C.T. Sims, N.S. Stoloff, and W.C. Hagel: *Superalloy II*, John Wiley & Sons Inc., New York, NY, 1987, pp. 255-61.
32. P.R. Bhowal, E.F. Wright, and E.L. Raymond: *Metall. Trans. A*, 1990, vol. 21, pp. 1709-17.
33. D. Mukherji, H. Gabrisch, W. Chen, H.J. Fecht, and R.P. Wahi: *Acta Mater*., 1997, vol. 45, pp. 3143-54.
34. J. Svoboda and P. Lukas: *Acta Mater*., 1997, vol. 45, pp. 125-35.
35. M. Feller–Kniepmier and T. Kuttner: *Acta Metall. Mater*., 1994, vol. 42, pp. 3167-74.
36. M. Probst–Hein, A. Dlouhy, and G. Eggeler: *Acta Mater*., 1999, vol. 47, pp. 2497-510.